

Investigation of the Crystallization Process of SAPO-35 and Si Distribution in the Crystals

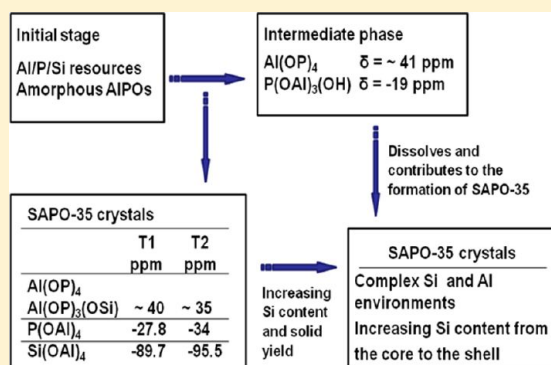
Peng Tian,[†] Bing Li,^{†,‡} Shutao Xu,[†] Xiong Su,^{†,‡} Dehua Wang,^{†,‡} Lin Zhang,[†] Dong Fan,^{†,‡} Yue Qi,[†] and Zhongmin Liu^{*,†}

[†]National Engineering Laboratory for Methanol to Olefins, Dalian National Laboratory for Clean Energy, Dalian Institute of Chemical Physics, Chinese Academy of Sciences, Dalian 116023, P. R. China

[‡]Graduate University of Chinese Academy of Sciences, Beijing 100049, P. R. China

S Supporting Information

ABSTRACT: The hydrothermal crystallization of SAPO-35 molecular sieve is examined in the present study. Many characterization methods including XRD, SEM, XRF, XPS, EDS, and various solid-state NMR techniques are applied to monitor the formation process of SAPO-35 and the development of the local environments of Si, P, and Al atoms as a function of crystallization time. The results show that an intermediate phase with ordered structure and AIPO compositions first forms. Subsequently, SAPO-35 crystallizes at the expense of the intermediate phase. Si takes part in the formation of SAPO-35 since the initial crystallization. The Si concentration in SAPO-35 shows an increasing trend with time, which leads to the change of both Si and Al coordination environments. More information is obtained from two-dimensional ²⁷Al MQ MAS and ²⁷Al → ³¹P MQ-MAS HETCOR NMR. Moreover, XPS analysis reveals the enrichment of Si on the crystal surface. On the basis of the characterization results, it is supposed that the distribution of Si in the SAPO-35 crystals is not uniform, showing a gradual increase from the core to the external surface.



1. INTRODUCTION

In the 1980s, the scientists at Union Carbide Corporation reported the synthesis of aluminophosphate (AIPO) and silicoaluminophosphate (SAPO) molecular sieves.^{1,2} The frameworks of AIPOs and SAPOs cover a range of different structure types; some are analogous to certain zeolites such as SAPO-35 (LEV structure), but a large number have unique structures without analogous zeolite. Since the frameworks of AIPO molecular sieves are neutral, they usually have no actual catalytic activities. The substitution of silicon into the framework of AIPOs, i.e. SAPOs, results in the appearance of acidity and leads to their catalytic application.^{3,4}

Up to now, synthesis of novel molecular sieves is mainly carried out by exploring synthetic parameters through trial and error, though some progress has been made in the past decade. Rational design and synthesis of molecular sieves with desired framework topologies and properties are the ideal way, which however requires a detailed understanding of the crystallization mechanism involved during the synthesis.^{4,5} Because molecular sieves are usually prepared by hydrothermal method from an amorphous gel containing organic amine as a structure-directing agent (SDA), the coexistence of multiple-component reactions and equilibrium in a heterogeneous environment causes the process extremely complex and makes the study on crystallization difficult. There exist two mechanisms regarding the crystallization process.^{6–8} One is the solution-mediated

transport mechanism involving dissolution of reagents followed by transport mechanisms to the nucleation sites where the crystal growth takes place, and another is the solid hydrogel transformation mechanism involving reorganization of the solid phase from amorphous components to crystalline. Cundy et al. once reviewed the crystallization mechanism of hydrothermal zeolite synthesis and claimed that the process can be most adequately explained by a mechanism based upon the solution-mediation mode, whether or not there is a visible liquid phase.⁸

Many attempts have been made to explore the crystallization process of AIPO molecular sieves including AIPO-5,^{9–11} -11,^{12–15} -18,¹⁶ and -36.¹⁷ However, the research on SAPO molecular sieve is mainly focused on SAPO-34, which is due to its excellent catalytic performance in methanol-to-olefin (MTO) reaction. Vistad et al. studied the hydrothermal crystallization of SAPO-34 using morpholine as the template in the presence of HF.^{18–20} They suggested that the gel first dissolved into 4-rings (4R) units, further constituting a layered intermediate (the prephase), and that the next steps were redissolution, nucleation, and crystallization of the prephase in different types of 4R building units. Huang and co-workers reinvestigated the above synthetic process with several solid-

Received: November 16, 2012

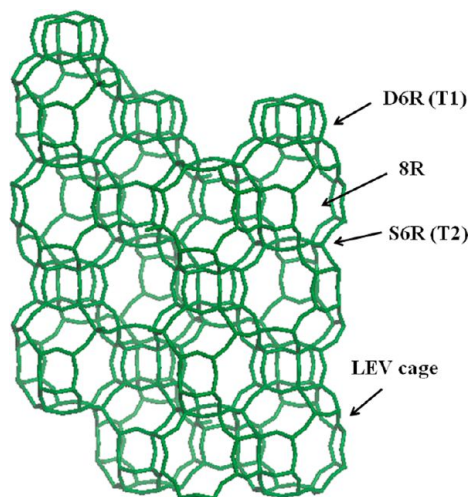
Revised: January 16, 2013

Published: January 29, 2013

state NMR techniques and focused on probing the local environments of P, Al, and Si as well as F^- in various solid phases formed during the synthesis.²¹ Huang et al. also studied that the crystallization of SAPO-34 by dry-gel conversion using diethylamine as the template.²² SAPO-34 crystallized from a semicrystalline precursor which had a layered structure held together by weak nonbonding interactions. Our group has reported the crystallization and Si incorporation mechanisms of SAPO-34 hydrothermally synthesized with triethylamine as the template, where the formation of SAPO-34 was ascribed to the contribution of a gel conversion mechanism.²³ Si directly participated in the crystallization since the initial stage and incorporated into the framework of SAPO-34 by SM2 (P substitution by Si) and SM3 (pairs of Al and P substitution by 2Si) mechanisms. In the following study on the crystallization process of SAPO-34 templated by diethylamine, we proposed a model of nonuniform Si distribution in the crystals with the increasing content from the core to the surface.²⁴ No semicrystalline precursor was observed during our investigations. From the above literatures, it can be seen that the evolution of crystallization may vary with the synthetic methods (hydrothermal synthesis or dry-gel conversion), even using the same organic template and with the same product. This is also supported by the crystallization of AlPO-11 synthesized with two different methods conducted by the same group.^{13,14}

SAPO-35 is a small-pore molecular sieve with eight member ring pore openings of 0.36×0.48 nm.²⁵ The structure of SAPO-35 is built by levyne cages, which are connected through single six rings (S6R) and double six rings (D6R) (Scheme 1).

Scheme 1. Framework of SAPO-35



There are two crystallographically distinct T sites in the framework: one in a D6R and other in a S6R. The distribution of these two sites is in the ratio of 2:1. Considering its interesting structures, SAPO-35 has been explored as CO_2 adsorbent and as catalyst for MTO reaction and methanol amination.^{26–28} Many research works have been reported about the synthesis optimization of SAPO-35.^{29,30} In the present work, we examine the crystallization process of SAPO-35 by using hexamethylenimine as a template. Attention is also given to the Si incorporation and Si distribution in the crystals. Many characterization techniques are employed to follow the SAPO-35 crystallization including XRD, SEM, XRF, XPS, EDS, and various solid-state NMR methods.

2. EXPERIMENTAL SECTION

2.1. Sample Preparation. SAPO-35 was hydrothermally synthesized from a gel composition of 1.35 hexamethylenimine (HMI):0.5 SiO_2 :1.0 Al_2O_3 :0.96 P_2O_5 :55 H_2O . The reagents used were pseudoboehmite (67.5% Al_2O_3), phosphoric acid (85%), and silica sol (28% SiO_2). Pseudoboehmite was added to the diluted phosphoric acid solution and stirred for 2 h until a uniform gel was obtained. Silica sol and the template HMI were added successively to the gel, which was stirred for 1 h to form a uniform reaction mixture. The gel was sealed in a 2 L autoclave and heated from ambient temperature to 473 K. Crystallization was carried out under autogenic pressure with stirring. The reaction mixture was withdrawn periodically from the autoclave during the synthesis process. The schematic diagram of synthesis apparatus is shown in Figure S1. The crystallization time was recorded since the start of heating from the room temperature. It took 0.95 and 1.25 h for the autoclave to reach 423 and 473 K, respectively. The liquid phase was separated from the solid phase by centrifugation. The wet solid was divided into two parts. One part was dried in air at room temperature. The other part was thoroughly washed with distilled water and dried at 393 K. The mother liquids obtained were evaporated at 393 K and then calcined at 923 K to measure the solid content.

SAPO-5 was hydrothermally synthesized from a gel composition of 1.2 triethylamine (TEA):0.4 SiO_2 :1.0 Al_2O_3 :1.0 P_2O_5 :60 H_2O . SAPO-11 was prepared with initial gel composition: 1.1 di-*n*-propylamine (DPA):0.4 SiO_2 :0.86 Al_2O_3 :1.0 P_2O_5 :55 H_2O . SAPO-34-TEA was prepared using TEA as template. The initial gel composition is 3.5TEA:0.3 SiO_2 :1.0 Al_2O_3 :1.0 P_2O_5 :55 H_2O .

2.2. Characterization. The powder XRD patterns of samples were collected on a PANalytical X'Pert PRO X-ray diffractometer with Cu $K\alpha$ radiation ($\lambda = 0.15406$ nm). The crystal morphology was characterized by scanning electron microscope (S-3400N Hitachi). The chemical composition of the samples was determined with a Philips Magix-601 X-ray fluorescence (XRF) spectrometer, and some samples were also analyzed by energy-dispersion X-ray spectrometer (EMAX Energy X-Max HORIBA) attached to SEM. The pH value of the synthetic gels was measured using a Mettler Toledo acid meter (Seven). XPS measurements were performed on a Thermo ESCALAB 250Xi spectrometer using Al $K\alpha$ radiation as the excitation source. Quantitative analysis of atomic ratios was accomplished by determining the elemental areas of the core-level peaks O 1s, Si 2p, Al 2p, and P 2p.

All the solid-state NMR experiments were performed on a Bruker AvanceIII 600 spectrometer equipped with a 14.1 T wide-bore magnet. The resonance frequencies were 156.4, 242.9, and 119.2 MHz for ^{27}Al , ^{31}P , and ^{29}Si , respectively. ^{27}Al and ^{31}P MAS NMR experiments were performed on a 4 mm MAS probe with a spinning rate of 13 kHz. ^{27}Al MAS NMR spectra were recorded using one pulse sequence. 200 scans were accumulated with a $\pi/8$ pulse width of 0.75 μs and a 2 s recycle delay. Chemical shifts were referenced to $(NH_4)_2Al(SO_4)_2 \cdot 12H_2O$ at -0.4 ppm. ^{31}P MAS NMR spectra were recorded using high-power proton decoupling. 100 scans were accumulated with a $\pi/4$ pulse width of 2.25 μs and a 4 s recycle delay. Chemical shifts were referenced to 85% H_3PO_4 at 0 ppm. ^{29}Si MAS NMR spectra were recorded with a 7 mm MAS probe with a spinning rate of 5 kHz using high-power proton decoupling. 5000–6000 scans were accumulated with a $\pi/4$

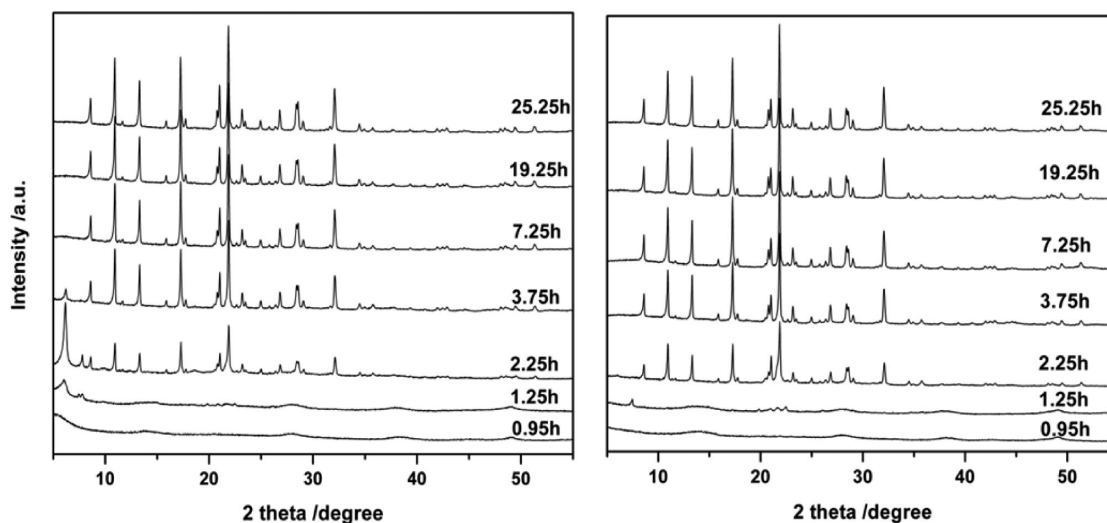


Figure 1. XRD patterns of the unwashed (left) and washed (right) samples with different crystallization times.

pulse width of 2.5 μ s and a 10 s recycle delay. Chemical shifts were referenced to 4,4-dimethyl-4-silapentanesulfonate sodium salt (DSS). $^1\text{H} \rightarrow ^{29}\text{Si}$ CP/MAS NMR experiment was carried out with a contact time of 3 ms and a recycle delay of 2 s.

The two dimension (2D) ^{27}Al MQ/MAS and $^{27}\text{Al} \rightarrow ^{31}\text{P}$ MQ-MAS HETCOR NMR experiments were performed on a 4 mm triple-channel MAS probe at a spinning speed of 13 kHz. ^{27}Al 3Q MAS NMR experiments were performed using a three-pulse sequence incorporating a z -filter.³¹ An rf field of 200 kHz was used for the creation ($0\text{Q} \rightarrow \pm 3\text{Q}$) and the first conversion ($\pm 3\text{Q} \rightarrow 0\text{Q}$) pulses. An rf field of 10 kHz was used for the last conversion step ($0\text{Q} \rightarrow \pm 1\text{Q}$), which was the central transition selective soft 90° pulse. A two-dimensional (2D) Fourier transformation followed by a shearing transformation gave a pure absorption mode 2D contour plot.^{31–33} The second-order quadrupolar effect (SOQE) and isotropic chemical shift (δ_{iso}) values were calculated according to the procedures in ref 31. The 2D $^{27}\text{Al} \rightarrow ^{31}\text{P}$ MQ-MAS HETCOR NMR spectra acquired using the sequence similar to ref 34. The preliminary triple-quantum excitation and conversion in the $^{27}\text{Al} \rightarrow ^{31}\text{P}$ MQ-MAS HETCOR sequence were achieved with an rf field of 200 kHz corresponding to pulse lengths of 5.2 and 1.7 μ s, respectively. The cross-polarization part of the sequence was carried out with a ^{31}P rf field of 21 kHz, a ^{27}Al rf field of 9 kHz, and a contact time of 3 ms. The spectra were acquired with 4800 scans for each of 128 experiments incrementing t_1 . The recycle delay of 0.2 s resulted in a total experimental time of 34.1 h.

3. RESULTS AND DISCUSSION

3.1. XRD and SEM. The powder XRD patterns of the as-synthesized samples with different crystallization times are shown in Figure 1. For the unwashed samples, the pattern of the sample heated for 0.95 h is similar to that of pseudoboehmite, indicating that most of the Al source has not reacted. After 1.25 h, though the broad reflections from pseudoboehmite still exist, there appears an obvious peak at 6.2° together with several weak peaks at 7.4° , 7.7° , and $18\text{--}23^\circ$. Upon washing, the peaks at 6.2° and 7.7° vanish completely, and the remaining reflections can be indexed to AlPO-5 phase.¹⁰ The peaks that disappeared are possibly due to a crystalline phase which has a layered structure held by weak

bonding interactions.^{13,22} Heating the gel for 2.25 h leads to the disappearance of AlPO-5 and the increase in the intensity of the peaks due to the layered phase. Meanwhile, there appear sharp peaks corresponding to the reflections of SAPO-35. Subsequently, SAPO-35 increases at the expense of the layered phase. After 3.75 h, only reflection peaks arising from SAPO-35 can be observed until the end of the crystallization.

The crystallization curve on the basis of relative crystallinity of the washed samples is plotted in Figure S2. The relative crystallinity rises with time and reaches 97% at $t = 7.25$ h. Afterward, the crystallinity of SAPO-35 is kept at high level with less change.

Figure 2 presents SEM images of the washed samples. Amorphous particles are observed in the 1.25 h sample. After heating for 2.25 h, large amount of rhombohedra crystals appear at the expense of amorphous materials, suggesting the crystallization of SAPO-35. Upon heating the gel for 7.25 h or longer, amorphous phase is invisible and only crystals are observed. Generally, SAPO-35 crystals grow larger and larger with the process of crystallization. SEM image of the unwashed sample with heating time of 2.25 h is also given in Figure 2. Only amorphous materials and rhombohedra crystals due to SAPO-35 are present in the image, indicating that the layered phase has an amorphous morphology.

3.2. XRF. The chemical compositions of the washed samples obtained by XRF are presented in Figure 3. The extremely high content of Al at the initial stage indicates that the amorphous materials observed by XRD and SEM are mainly from unreacted alumina. A maximum of Al content appears at $t = 1.25$ h, whereas the contents of both P and Si show the lowest values. This should be caused by the faster dissolution of P and Si sources than Al source into the solution. Afterward, the contents of P and Si in the samples rise with the rapid decrease of Al content until 3.75 h. According to the XRD results, the great change in elemental compositions of the samples during this period is ascribed to the dissolution of amorphous alumina and the formation of SAPO-35 involving the incorporation of Al, P, and Si. After 3.75 h, the change of solid compositions of the samples becomes much slow. Because the washed samples only contain SAPO-35 crystals after 7.25 h as revealed by SEM images, the XRF compositions of the washed samples are directly related to the bulk composition of SAPO-35 during the

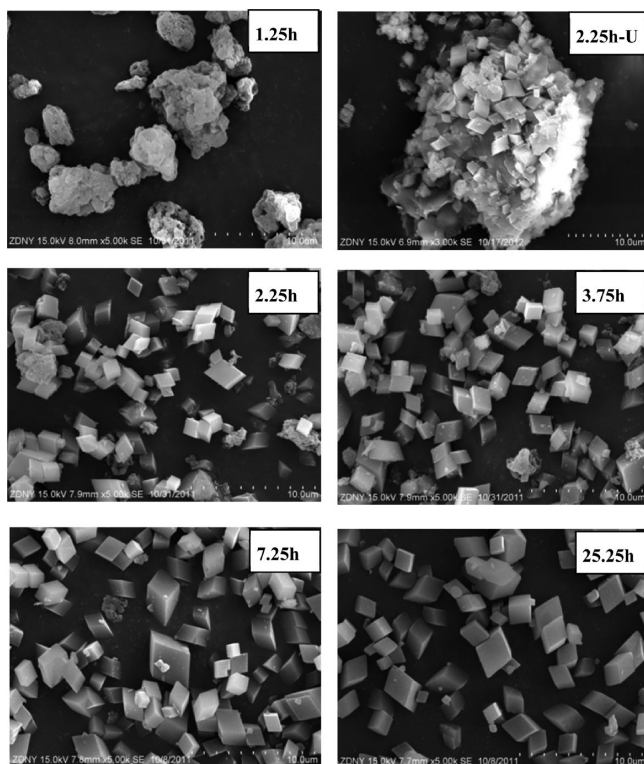


Figure 2. SEM images of the as-synthesized samples with different crystallization times. All samples are washed except 2.25h-U (the unwashed 2.25 h sample).

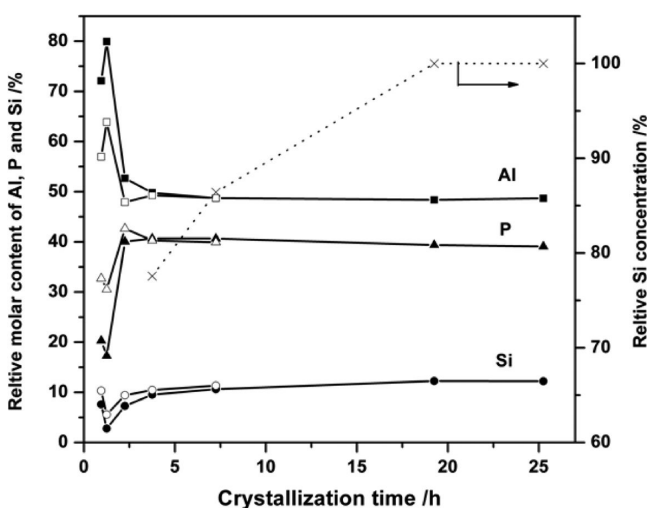


Figure 3. Chemical compositions of the unwashed (hollow) and washed (solid) samples. The relative Si concentration in SAPO-35 crystals is also shown in the figure (dotted line), which is defined as $(n_{\text{Si}}/n_{\text{Si+Al+P}})_t / (n_{\text{Si}}/n_{\text{Si+Al+P}})_{25.25 \text{ h}}$.

period of 7.25–25.25 h. In addition, the relative Si concentration in SAPO-35 crystals, defined as $(n_{\text{Si}}/n_{\text{Si+Al+P}})_t / (n_{\text{Si}}/n_{\text{Si+Al+P}})_{25.25 \text{ h}}$, is also plotted in Figure 3. The value at 3.75 h is roughly calculated by assuming only SAPO-35 crystals contained in the washed sample. Clearly, the Si content in SAPO-35 grows with time to reach 100% at 19.25 h and keeps unchanged until the end of the crystallization.

The XRF results of the unwashed samples are also shown in Figure 3. Both the unwashed and washed samples show similar trends in elemental compositions with the crystallization time.

The differences between these two serial samples, especially before 3.75 h, are possibly caused by the following reasons: (1) the amorphous Al_2O_3 in the solid samples which absorbs large quantities of soluble P and Si sources; (2) the existence of soluble layered phase.

3.3. Solid Contents and pH of the Mother Liquids.

Figure 4 gives the change of the solid contents and pH values of

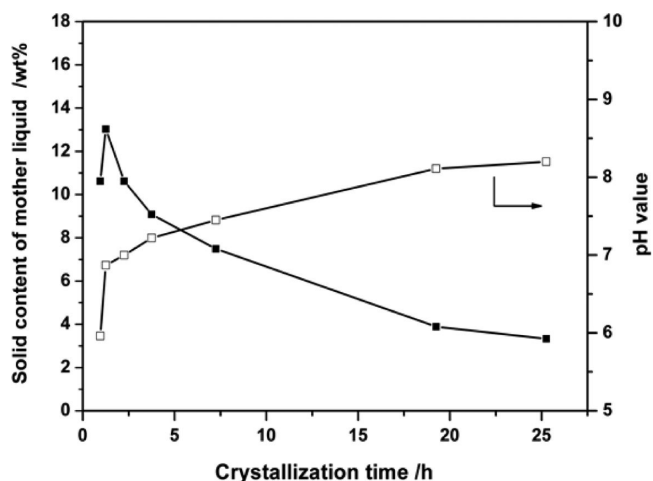


Figure 4. Solid content and pH value of mother liquids.

the mother liquids following the evolution of crystallization. The solid content of the liquid shows an obvious volcano with a maximum of 13 wt % at $t = 1.25$ h. Afterward, the solid content drops with time and reaches a value of 3.3 wt % at the end of crystallization. In combination with the results from XRD and XRF, the appearance of the maximum in solid content at the early stage is ascribed to the fast dissolution of sources into the liquid, whereas the subsequent decrease mainly results from the gradual formation of crystalline products.

The pH value of the mother liquid rises with time during the whole crystallization. This should be caused by the consumption of H_3PO_4 , which reacts with Al_2O_3 particles and prompts the dissolution of Al source. Moreover, part of the organic amine initially combined with H_3PO_4 would be gradually released following the progress of crystallization and also contribute to the pH increase of the mother liquid.

3.4. NMR Characterization. To characterize the local environments of P, Al, and Si atoms in the samples, solid-state NMR experiments were performed. Figure 5 presents the ^{31}P MAS NMR spectra of the unwashed and washed samples. The spectrum of the unwashed sample at $t = 0.95$ h exhibits a broad peak centered at around -8.1 ppm. This extreme broadness of the peak reflects the amorphous nature of the gel sample as shown in the XRD pattern. It is attributed to the P sites in the amorphous aluminophosphate materials. For the unwashed sample heated for 1.25 h, the broad peak becomes weak, and there emerge a sharp peak at -18.9 ppm and a weak one at -27.8 ppm. The sharp peak, disappearing after washing the sample, is ascribed to the P species in the layered material. Its narrow peak width indicates the ordered local environment around P atom in the layered phase, though the P is not fully condensed, as judging from its chemical shift.¹³ The peak at -27.8 ppm corresponds to the $\text{P}(\text{OAl})_4$ species, resulting from the formation of small amount of AlPO_5 .⁹ The P spectrum of the unwashed sample heated for 2.25 h shows that the peak at -27.8 ppm becomes intensified and one additional peak at -34

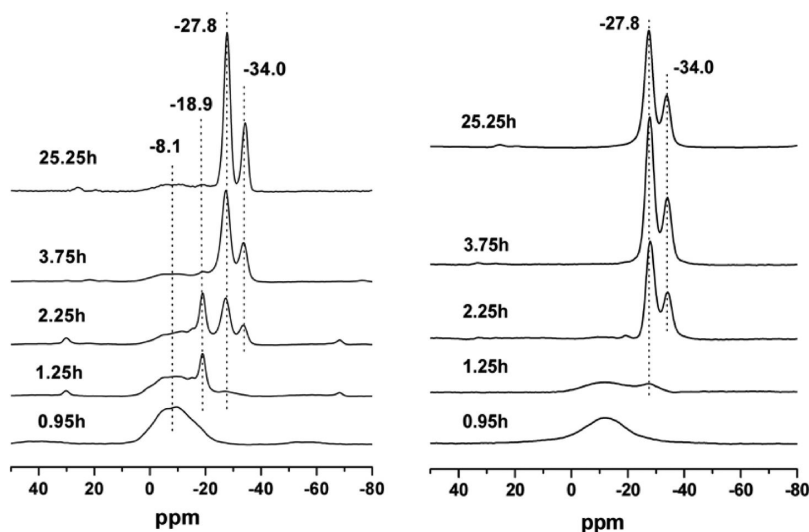


Figure 5. ^{31}P MAS NMR spectra of the unwashed (left) and washed (right) samples.

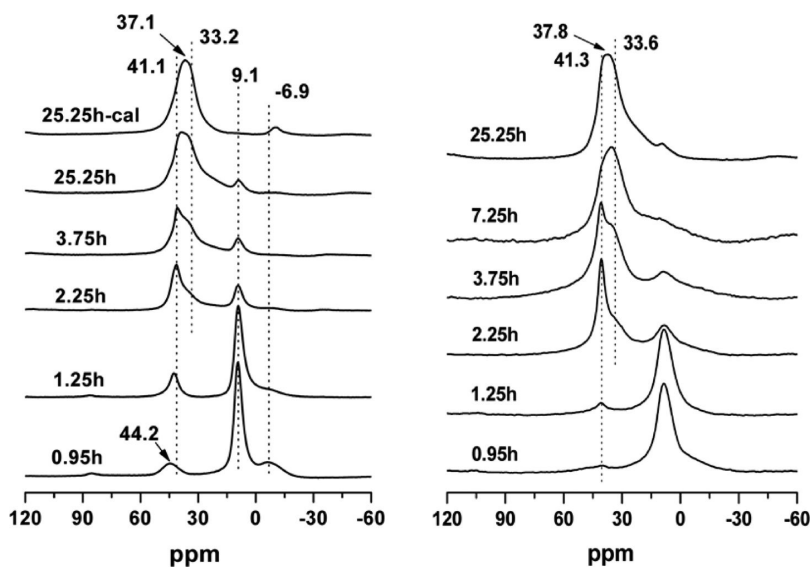


Figure 6. ^{27}Al MAS NMR spectra of the unwashed (left) and washed (right) samples.

ppm appears. In combination with the XRD results, these two peaks are attributed to the $\text{P}(\text{OAl})_4$ species in the framework of SAPO-35 with two different crystallographical T sites.³⁵ The deconvoluted analysis of the spectrum of the washed sample shows that the two sites have a ratio of $P_{\text{T1}(-27.8 \text{ ppm})}/P_{\text{T2}(-34 \text{ ppm})} = 1.92$, close to the theoretical value of 2. For the unwashed sample of 3.75 h, the intensity of the peaks due to SAPO-35 increases at the expense of the signals at -8.1 and -18.9 ppm, implying the decreasing amount of amorphous material and layered phase in the solid. A weak resonance due to the amorphous P species is still apparent in the spectrum of the unwashed 25.25 h sample, which should be from the mother liquid contained in the sample. Upon washing, only the P species from SAPO-35 are observed since 3.75 h. Overall, the changes in the P environments are parallel to these obtained in the XRD.

The ^{27}Al MAS NMR spectra are shown in Figure 6. The spectrum of the unwashed sample at 0.95 h exhibits three peaks at 44.2 (weak), 9.1 (strong), and -6.9 ppm (weak). The strong peak at 9.1 ppm should be due to the large amount of

unreacted alumina source. The peaks at 44.2 and -6.9 ppm are ascribed to the tetrahedral Al and the octahedral Al with an $\text{Al}(\text{OP})_4(\text{OH})_2$ environment in the AlPO-based materials, respectively.¹³ Both peaks become weak in the spectrum of the washed sample, indicating the solubility of two Al species. For the unwashed sample heating for 2.25 h, the peak at 44.2 ppm shifts to higher field and grows intensely together with the emergence of a shoulder at 33.2 ppm, whereas the intensities of the other two signals greatly decrease. Less change in the spectrum occurs after washing the sample except the sharpness of the peak at 41.3 ppm. It is not apparent from the spectrum if the two peaks at ca. 41 and 33 ppm originate from tetrahedral Al species in SAPO-35 with the crystallographic non-equivalence or a combination of Al species from SAPO-35 and the layered phase. Heating the gel for 3.75 h or longer results in the gradual increase of the shoulder signal, which can be seen more clearly in the spectra of the washed samples. One broad and asymmetric peak centered at ca. 37 ppm arising from SAPO-35 is observed in the spectrum of the 25.25 h sample together with a weak signal at 9.1 ppm. This weak signal

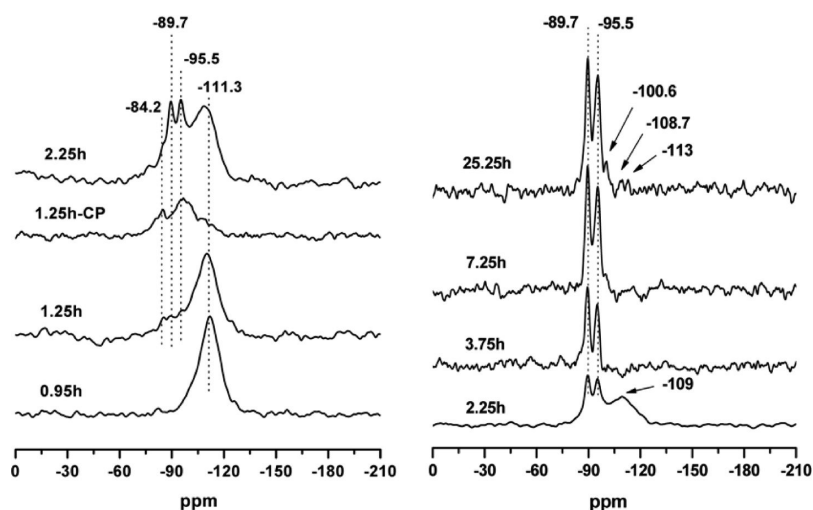


Figure 7. ^{29}Si MAS NMR spectra of the unwashed (left) and washed (right) samples. 1.25h-CP stands for the $^1\text{H} \rightarrow ^{29}\text{Si}$ CP MAS NMR spectrum of the unwashed 1.25 h sample.

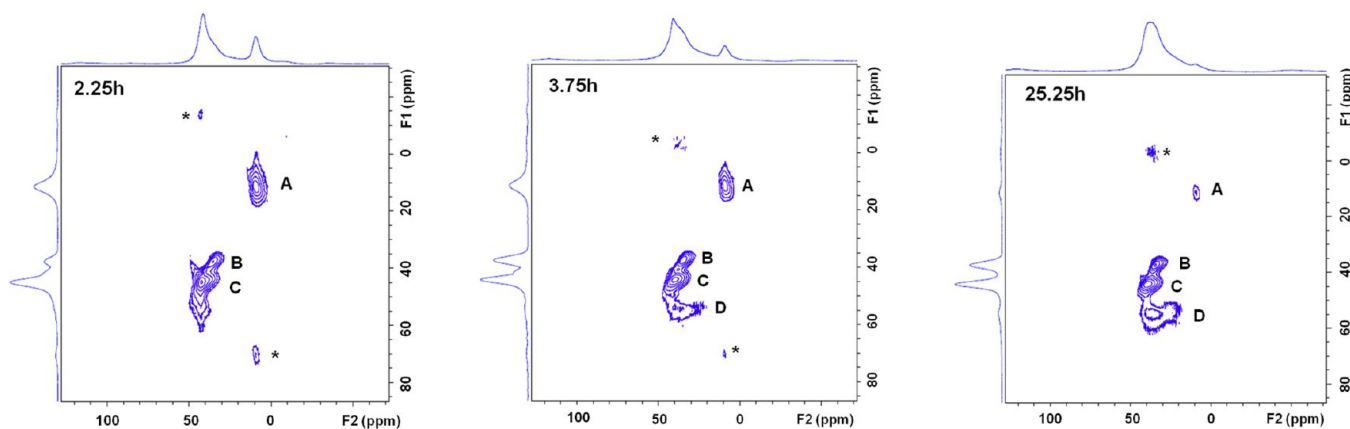


Figure 8. ^{27}Al MQ MAS NMR spectra of the unwashed samples. Spinning sideband is denoted with an asterisk.

disappears after calcining the sample (Figure 6, 25.25h-cal) and therefore corresponds to the pentacoordinated Al species in SAPO-35. However, because SAPO-35 is the unique crystalline product in the washed samples since 2.25 h, it is unclear why the relative intensities of the peaks due to the tetraordinated Al in SAPO-35 show obvious change with the crystallization time. Further study is needed to resolve the complicated Al peaks.

The ^{29}Si MAS NMR spectra of selected samples are obtained to follow the Si incorporation during the crystallization (Figure 7). One broad resonance centered at -111.3 ppm is observed in the spectrum of the unwashed 0.95 h sample, which can be assigned to amorphous Si with $\text{Si}(\text{OSi})_4$ environments.²² Several small peaks (-83 to -97 ppm) start to emerge after heating the gel for 1.25 h. The $^1\text{H} \rightarrow ^{29}\text{Si}$ CP MAS NMR of this sample is carried out to clarify the origin of these resonances. As shown in Figure 7 (1.25h-CP), the peak at ca. -97.0 ppm becomes dominant together with two shoulders at -110 and -84.2 ppm. The weak CP signal arising from amorphous silica is consistent with that this species contains less silanol groups. According to the literature,^{22,36} the signal at -97.0 ppm corresponds to $\text{Si}(\text{OSi})_2(\text{OH})_2$ or $\text{Si}(\text{OSi})_2(\text{OAl})(\text{OH})$ and the signal at -84.2 ppm should arise from $\text{Si}(\text{OAl})_3(\text{OH})$ or $\text{Si}(\text{OSi})(\text{OAl})_2(\text{OH})$ environments, indicating the existence of amorphous aluminosilicate species and

silica species with low polymerization degree in the sample. The protons on the silanol groups are the reason that the intensities of these Si signals are enhanced in the CP spectrum. Heating the gel for 2.25 h yields two sharp peaks centered at -89.7 and -95.5 ppm besides the resonance at -109 ppm. The appearance of the two signals, which remain after washing, agrees with the crystallization of SAPO-35 as revealed by XRD and SEM. They are assigned to the $\text{Si}_{\text{T}1}(\text{OAl})_4$ and $\text{Si}_{\text{T}2}(\text{OAl})_4$ species in the framework of SAPO-35, respectively.³⁵ Moreover, these results also imply that the layered phase is mainly AlPO in nature, which contains less Si in the framework. In order to clearly observe the Si incorporation and avoid the disturbing of amorphous Si, Si spectra of the washed samples are recorded since the formation of SAPO-35. It can be seen that only signals arising from $\text{Si}(\text{OAl})_4$ of SAPO-35 exist in the spectrum of the washed 3.75 h sample. A new weak peak at -100.6 ppm emerges at 7.25 h, which corresponds to the formation of 5Si islands in the framework.^{37,38} At the end of crystallization, more signals appear in the spectrum, suggesting the generation of 8Si or larger islands. The change in Si environments is consistent with the increasing Si content in the samples with time as shown in XRF. However, an exact assignment of these resonances is difficult due to the existence of two T sites in the framework.³⁵

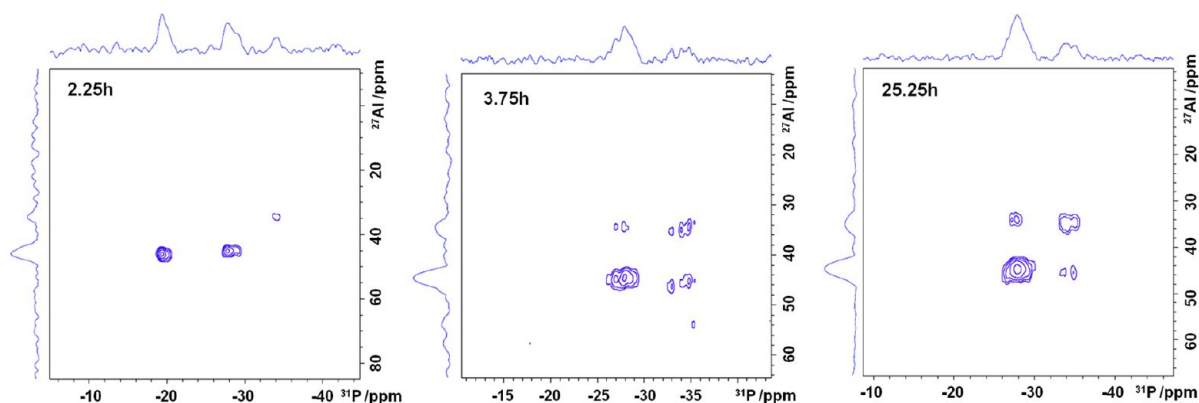


Figure 9. $^{27}\text{Al} \rightarrow ^{31}\text{P}$ MQ-MAS HETCOR spectra of the unwashed samples.

3.5. ^{27}Al MQ MAS NMR and $^{27}\text{Al} \rightarrow ^{31}\text{P}$ MQ-MAS HETCOR NMR. The 2D multi-quantum (MQ) MAS NMR technique can effectively refocus the second-order anisotropic broadening and give isotropic spectra along the F1 dimension, whereas the F2 dimension exhibits the normal second-order quadrupolar line shapes. The ^{27}Al MQ MAS spectra of three selected samples are illustrated in Figure 8. The detailed isotropic shifts and second-order quadrupolar effect parameter (SOQE) of each signal in the spectra are shown in Table S1. Four signals labeled as A, B, C, and D are observed in the spectra of 3.75 and 25.25 h samples, whereas three signals for the 2.25 h sample. For all three spectra, signal A has an isotropic shift of ~ 10.6 ppm due to pentacoordinated Al species in the sample; signals B, C, and D, arising from tetrahedral Al with different environments, show gradually increasing isotropic shifts and SOQE values, except the close SOQE for B and C in the spectrum of the 2.25 h sample. Normally, for SAPO molecular sieves, the increase of SOQE reflects the decreasing symmetry around tetrahedral Al atoms in the framework, which results from the gradual substitution of P by Si in the second coordination sphere of Al.^{39,40} However, the existence of two T sites in the framework of SAPO-35 makes the assignment of signals B–D complex.

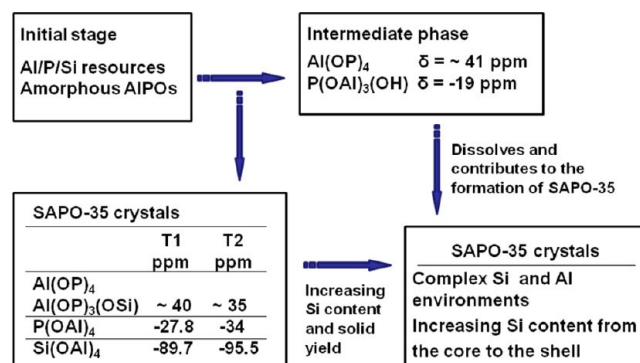
The $^{27}\text{Al} \rightarrow ^{31}\text{P}$ MQ-MAS HETCOR spectra are further performed to obtain the detailed information on the connectivity between Al and P atoms, which would be helpful to make a clear assignment of signals in the Al spectra (Figure 9). Because CP process is sensitive to the internuclear distance, only the ^{31}P nuclei that are in the close vicinity of Al atoms will be detected. In the present study, isotropic dimension in the ^{27}Al MQ MAS is used to do the two-dimensional experiment due to its better resolution for Al species.³⁴ For the 25.25 h unwashed sample, the P projection contains two resonances at -27 ($\text{P}_{\text{T}2}$) and -33 ppm ($\text{P}_{\text{T}2}$), corresponding to those seen in the ^{31}P MAS spectrum. Both $\text{P}_{\text{T}1}$ and $\text{P}_{\text{T}2}$ sites correlate with two tetrahedral Al sites (37 and 44 ppm) in the Al projection, and a very strong correlation is observed between $\text{P}_{\text{T}1}$ and the Al site at 44 ppm. According to the topology of LEV, the second coordination spheres of the two nonequivalent P sites can be expressed as $\text{P}_{\text{T}1}$ ($3\text{Al}_{\text{T}1}$, $1\text{Al}_{\text{T}2}$) and $\text{P}_{\text{T}2}$ ($2\text{Al}_{\text{T}1}$, $2\text{Al}_{\text{T}2}$), respectively. Therefore, the resonances at 37.3 and 44.3 ppm in the Al projection, corresponding to the signals B and C in the ^{27}Al MQ MAS, are ascribed to $\text{Al}_{\text{T}2}$ and $\text{Al}_{\text{T}1}$ sites in the framework, respectively. The weak resonance at 54.6 ppm corresponding to signal D in the ^{27}Al MQ MAS does not appear in the Al projection. Considering its high isotropic shift

and large SOQE, the signal D is attributed to the tetrahedral Al with more connectivity with Si in the second coordination sphere, though its crystallographic position is not clear. A similar correlation map between P and Al atoms is found for the 3.75 h sample. The HETCOR spectrum of the 2.25 h sample shows three peaks at -19 , -27 ($\text{P}_{\text{T}1}$), and -33 ppm ($\text{P}_{\text{T}2}$) in the P projection. The P site centered at -19 ppm correlates with the tetrahedral Al at 45 ppm, which corresponds to the signal at ~ 41 ppm in the 1D spectrum. This indicates that the layered phase consists of tetrahedral P and Al. Part of correlations between P and Al sites of the SAPO-35 framework do not appear in the 2.25 h spectrum due to the low amount of SAPO-35 in the sample of this moment.

On the basis of the above results, the signals B, C, and D in the ^{27}Al MQ NMR spectra are assigned to $\text{Al}_{\text{T}2}(\text{OP})_n(\text{OSi})_{(4-n)}$ ($n = 4$ or 3), $\text{Al}_{\text{T}1}(\text{OP})_n(\text{OSi})_{(4-n)}$ ($n = 4$ or 3), and $\text{Al}(\text{OP})_n(\text{OSi})_{(4-n)}$ ($n = 0-2$) (Table S1). Moreover, because the Si content in SAPO-35 gradually increases and the Si environment becomes complex with time, it is speculated that the percentage of signal D in B–D rises following the evolution of crystallization, which thus causes the change of the peak shape of the tetrahedral Al in the ^{27}Al NMR spectra.

3.6. Crystallization Process. According to the above characterization results, the crystallization process of SAPO-35 can be pictured (Scheme 2). In the initial stage of crystallization ($t \leq 0.95$ h), part of P, Si, and Al sources dissolve into the liquid, and the solid is composed of small amount of amorphous AlPOs and unreacted alumina and silica. A crystalline material with layered phase and AlPO compositions appears after heating the gel for 1.25 h. SAPO-35 is observed in

Scheme 2. Illustration of the Crystallization Process of SAPO-35



the 2.25 h sample. Subsequently, the relative crystallinity of SAPO-35 rises with time at the expense of layered phase. At 7.25 h, both the layered phase and amorphous materials disappear, and the product becomes pure SAPO-35 crystals. Considering the good crystallinity of the layered phase and the difference in Si content between layered phase and SAPO-35, it is supposed that the layered phase dissolves into the liquid and further contributes to the formation of SAPO-35. The nutrition for the growth of SAPO-35, such as Al, P, and Si elements, comes from the liquid. The solid yield of SAPO-35 increases with time until the end of the crystallization.

3.7. Si Incorporation Mechanism and Si Distribution in the Crystals. The results of ^{29}Si , ^{27}Al , ^{31}P NMR, and XRF imply that Si directly participates in the formation of the framework of SAPO-35 since the initial crystallization. Si substitutes for P first to generate the $\text{Si}(\text{OAl})_4$ environment (SM II), and then a combination of SM II and SM III (2Si for the pairs of P and Al) mechanisms leads to the formation of Si islands in SAPO-35 crystals.

XPS experiment is performed to study the surface composition of SAPO-35 crystals (the washed 25.25 h sample). The result is shown in Table 1. Clearly, the Si content on the

Table 1. Bulk and Surface Compositions of SAPO Molecular Sieves

sample	elemental composition (mol %)		$\text{Si}_{\text{surface}}/\text{Si}_{\text{bulk}}$
	XRF	XPS	
SAPO-11	$\text{Si}_{0.045}\text{Al}_{0.498}\text{P}_{0.458}$	$\text{Si}_{0.224}\text{Al}_{0.462}\text{P}_{0.314}$	4.98
SAPO-5	$\text{Si}_{0.073}\text{Al}_{0.488}\text{P}_{0.439}$	$\text{Si}_{0.155}\text{Al}_{0.420}\text{P}_{0.424}$	2.12
SAPO-34-TEA	$\text{Si}_{0.080}\text{Al}_{0.486}\text{P}_{0.434}$	$\text{Si}_{0.206}\text{Al}_{0.453}\text{P}_{0.341}$	2.58
SAPO-34-DEA ^a	$\text{Si}_{0.164}\text{Al}_{0.478}\text{P}_{0.358}$	$\text{Si}_{0.231}\text{Al}_{0.440}\text{P}_{0.329}$	1.41
SAPO-35-25.25h	$\text{Si}_{0.122}\text{Al}_{0.488}\text{P}_{0.390}$	$\text{Si}_{0.187}\text{Al}_{0.478}\text{P}_{0.335}$	1.53
	$\text{Si}_{0.149}\text{Al}_{0.470}\text{P}_{0.381}^b$	$\text{Si}_{0.153}\text{Al}_{0.464}\text{P}_{0.383}^b$	
	$\text{Si}_{0.153}\text{Al}_{0.477}\text{P}_{0.371}^b$	$\text{Si}_{0.148}\text{Al}_{0.469}\text{P}_{0.383}^b$	
SAPO-35-2.25h	$\text{Si}_{0.098}\text{Al}_{0.496}\text{P}_{0.405}^b$	$\text{Si}_{0.101}\text{Al}_{0.484}\text{P}_{0.415}^b$	
	$\text{Si}_{0.106}\text{Al}_{0.481}\text{P}_{0.413}^b$	$\text{Si}_{0.100}\text{Al}_{0.492}\text{P}_{0.408}^b$	

^aData from ref 24. SAPO-34-DEA was synthesized with DEA as template. ^bElemental compositions of SAPO-35 crystals from EDS analysis. Data of samples at each crystallization time were obtained from randomly selected four crystals.

surface is higher than that in the bulk, indicating the enrichment of Si on the crystal surface. The elemental composition of SAPO-35 is also investigated by SEM-EDS (Table 1). Similar surface compositions are found among crystals of one sample, and the Si content on the surface of SAPO-35 increases with time, which is consistent with the XRF results. The increasing Si concentration in SAPO-35 should be related to the pH increase of the synthetic gel following the crystallization, which facilitates the depolarization of colloid silica and promotes the incorporation degree of Si into the framework.

On the basis of the information from XRF, XPS, and SEM-EDS, it is proposed that the distribution of Si in the crystal is not uniform, showing a gradual increase from the core to the external surface. This means that the local environments of Si atoms in the crystals with higher Si content are also not homogeneous: Si (4Al) in the crystal center and coexistence of multiple $\text{Si}(\text{OAl})_n$ ($n = 0-4$) environments at the edge of the crystal. This is similar to what we have found in SAPO-34 crystals templated by diethylamine.²⁴ Moreover, the increase of solid yields and the heterogeneity of crystal sizes shown by

SEM suggest the occurrence of secondary nucleation during the crystallization process. The newly formed crystals, possessing higher Si content in the core as compared with that of the original crystals, also have an increasing Si content from the core to the surface.

Considering that pH value normally shows an increasing trend in the hydrothermal synthesis of SAPO molecular sieves,^{20,41,42} the nonuniform distribution of Si in the crystals is possibly a common feature for SAPO molecular sieves. Therefore, several SAPO molecular sieves are hydrothermally synthesized and characterized by XPS (Table 1). It is found that all samples exhibit the Si enrichment phenomenon on the crystal surface, supporting the speculation well. Interestingly, SAPO-11 shows a relatively high ratio of $\text{Si}_{\text{surface}}$ to Si_{bulk} , implying that the core of the SAPO-11 crystals is much deficient in Si. This should be related to its specific framework topology besides the influence of pH value of the synthetic gel.

4. CONCLUSIONS

The crystallization process of SAPO-35 has been investigated in detail. An intermediate phase with ordered structure and AlPO compositions crystallizes first and then coexists with SAPO-35 at the crystallization period of $t \leq 3.75$ h. Subsequently, the intermediate phase gradually dissolves and the product becomes pure SAPO-35 crystals since 7.25 h. The nutrition for the growth of SAPO-35, such as Al, P, and Si elements, comes from the liquid. Si directly participates in the formation of SAPO-35 in the initial crystallization. The Si concentration in SAPO-35 rises with time due to the pH increase of the synthetic gel, which promotes the dissolution of silica source and improves the Si incorporation into the framework. Multiple Si environments appear in the framework of SAPO-35 with a higher Si content. The coordination environment of Al atom is also modified by the increasing Si content. The concentration of $\text{Al}(\text{OP})_n(\text{OSi})_{(4-n)}$ ($n = 0-2$) species in SAPO-35 rises at the expense of $\text{Al}(\text{OP})_n(\text{OSi})_{(4-n)}$ ($n = 4$ or 3) and thus causes an obvious change in the Al spectra. In addition, there exists a Si enrichment phenomenon on the surface of SAPO-35. The distribution of Si in the SAPO-35 crystals is not homogeneous, rising gradually from the core to the surface. Further study indicates that the nonuniform distribution of Si in the crystals is possibly a common feature for the SAPO molecular sieves synthesized by the hydrothermal method.

■ ASSOCIATED CONTENT

● Supporting Information

Schematic diagram of the apparatus for synthesis, crystallization curve, and table of chemical shifts and SOQE parameters of the unwashed samples from the ^{27}Al MQ MAS NMR spectra. This material is available free of charge via the Internet at <http://pubs.acs.org>.

■ AUTHOR INFORMATION

Corresponding Author

*Ph +86-411-84379335; e-mail liuzm@dicp.ac.cn.

Notes

The authors declare no competing financial interest.

■ ACKNOWLEDGMENTS

We are grateful for the financial support from the National Natural Science Foundation of China (NSFC 21101150 and NSFC 21103180).

REFERENCES

- (1) Wilson, S. T.; Lok, B. M.; Messina, C. A.; Cannan, T. R.; Flanigen, E. M. Aluminophosphate Molecular Sieves: a New Class of Microporous Crystalline Inorganic Solids. *J. Am. Chem. Soc.* **1982**, *104*, 1146–1147.
- (2) Lok, B. M.; Messina, C. A.; Patton, R. L.; Gajek, T. R.; Cannan, T. R.; Flanigen, E. M. Silicoaluminophosphate Molecular Sieves: Another New Class of Microporous Crystalline Inorganic Solids. *J. Am. Chem. Soc.* **1984**, *106*, 6092–6093.
- (3) Wright, P. A. *Microporous Framework Solids*; RSC Publishing: Cambridge, UK, 2007.
- (4) Yu, J.; Xu, R. Insight into the Construction of Open-Framework Aluminophosphates. *Chem. Soc. Rev.* **2006**, *35*, 593–604.
- (5) Wang, Z.; Yu, J.; Xu, R. Needs and Trends in Rational Synthesis of Zeolitic Materials. *Chem. Soc. Rev.* **2012**, *41*, 1729–1741.
- (6) Francis, R. J.; O'Hare, D. The Kinetics and Mechanisms of the Crystallisation of Microporous Materials. *J. Chem. Soc., Dalton Trans.* **1998**, 3133–3148.
- (7) Uzcátegui, D.; González, G. Study of the Kinetics of Crystallization of Zeolite MEL. *Catal. Today* **2005**, *107–108*, 901–905.
- (8) Cundy, C. S.; Cox, P. A. Precursors, Intermediates and Reaction Mechanism. *Microporous Mesoporous Mater.* **2005**, *82*, 1–78.
- (9) Longstaffe, J. G.; Chen, B.; Huang, Y. Characterization of the Amorphous Phases Formed During the Synthesis of Microporous Material AlPO₄-5. *Microporous Mesoporous Mater.* **2007**, *98*, 21–28.
- (10) Chen, B.; Kirby, C. W.; Huang, Y. Investigation of Crystallization of Molecular Sieve AlPO₄-5 by the Dry Gel Conversion Method. *J. Phys. Chem. C* **2009**, *113*, 15868–15876.
- (11) Fan, F.; Feng, Z.; Sun, K.; Guo, M.; Guo, Q.; Song, Y.; Li, W.; Li, C. In Situ UV Raman Spectroscopic Study on the Synthesis Mechanism of AlPO₄-5. *Angew. Chem., Int. Ed.* **2009**, *48*, 8743–8747.
- (12) Zhang, B.; Xu, J.; Fan, F.; Guo, Q.; Tong, Z.; Yan, W.; Yu, J.; Deng, F.; Li, C.; Xu, R. Molecular Engineering of Microporous Crystals: (III) The Influence of Water Content on the Crystallization of Microporous Aluminophosphate AlPO₄-11. *Microporous Mesoporous Mater.* **2012**, *147*, 212–221.
- (13) Chen, B.; Huang, Y. Examining Self-Assembly of Microporous Materials, AlPO₄-11, by Dry Gel Conversion. *J. Phys. Chem. C* **2007**, *111*, 15236–15243.
- (14) Huang, Y.; Richer, R.; Kirby, C. W. A Study of the Formation of Molecular Sieve SAPO-44. *J. Phys. Chem. B* **2003**, *107*, 1326–1337.
- (15) Cheng, T.; Xu, J.; Li, X.; Li, Y.; Zhang, B.; Yan, W.; Yu, J.; Sun, H.; Deng, F.; Xu, R. Molecular Engineering of Microporous Crystals: (IV) Crystallization Process of Microporous Aluminophosphate AlPO₄-11. *Microporous Mesoporous Mater.* **2012**, *152*, 190–207.
- (16) Huang, Y.; Demko, B. A.; Kirby, C. W. Investigation of the Evolution of Intermediate Phases of AlPO₄-18 Molecular Sieve Synthesis. *Chem. Mater.* **2003**, *15*, 2437–2444.
- (17) Xu, J.; Zhou, D.; Song, X.; Chen, L.; Yu, J.; Ye, C.; Deng, F. Crystallization of Magnesium Substituted Aluminophosphate of Type-36 as Studied by Solid-State NMR Spectroscopy. *Microporous Mesoporous Mater.* **2008**, *115*, 576–584.
- (18) Vistad, Ø. B.; Hansen, E. W.; Akporiaye, D. E.; Lillerud, K. P. Multinuclear NMR Analysis of SAPO-34 Gels in the Presence and Absence of HF: The Initial Gel. *J. Phys. Chem. A* **1999**, *103*, 2540–2552.
- (19) Vistad, Ø. B.; Akporiaye, D. E.; Lillerud, K. P. Identification of a Key Precursor Phase for Synthesis of SAPO-34 and Kinetics of Formation Investigated by in Situ X-ray Diffraction. *J. Phys. Chem. B* **2001**, *105*, 12437–12447.
- (20) Vistad, Ø. B.; Akporiaye, D. E.; Taulelle, F.; Lillerud, K. P. In Situ NMR of SAPO-34 Crystallization. *Chem. Mater.* **2003**, *15*, 1639–1649.
- (21) Yan, Z.; Chen, B.; Huang, Y. A solid-State NMR Study of the Formation of Molecular Sieve SAPO-34. *Solid State Nucl. Magn. Reson.* **2009**, *35*, 49–60.
- (22) Zhang, L.; Bates, J.; Chen, D.; Nie, H.; Huang, Y. Investigation of Formation of Molecular Sieve SAPO-34. *J. Phys. Chem. C* **2011**, *115*, 22309–22319.
- (23) Tan, J. L. J.; Bao, X.; Liu, X.; Han, X.; He, C.; Zhai, R. Crystallization and Si Incorporation Mechanisms of SAPO-34. *Microporous Mesoporous Mater.* **2002**, *53*, 97–108.
- (24) Liu, G. Y.; Tian, P.; Zhang, Y.; Li, J. Z.; Xu, L.; Meng, S. H.; Liu, Z. M. Synthesis of SAPO-34 Templated by diethylamine: Crystallization Process and Si Distribution in the Crystals. *Microporous Mesoporous Mater.* **2008**, *114*, 416–423.
- (25) <http://www.iza-structure.org/databases/>.
- (26) Cheung, O.; Liu, Q.; Bacsik, Z.; Hedin, N. Silicoaluminophosphates as CO₂ Sorbents. *Microporous Mesoporous Mater.* **2012**, *156*, 90–96.
- (27) Jeon, H.-Y.; Shin, C.-H.; Jung, H. J.; Hong, S. B. Catalytic Evaluation of Small-Pore Molecular Sieves with Different Framework Topologies for the Synthesis of Methylamines. *Appl. Catal., A* **2006**, *305*, 70–78.
- (28) Zhu, Z.; Hartmann, M.; Kevan, L. Catalytic Conversion of Methanol to Olefins on SAPO-n (n = 11, 34 and 35) CrAPSO-n and Cr-SAPO-n Molecular Sieves. *Chem. Mater.* **2000**, *12*, 2781–2787.
- (29) Venkatathri, N.; Yoo, J. W. Synthesis, Characterization and Catalytic Properties of a LEV Type Silicoaluminophosphate Molecular Sieve, SAPO-35 from Aqueous Media Using Aluminium Isopropoxide and Hexamethylenimine Template. *Appl. Catal., A* **2008**, *340*, 265–270.
- (30) Venkatathri, N. Synthesis and Characterization of High Silica Content Silicoaluminophosphate SAPO-35 from Non-aqueous Medium. *Catal. Commun.* **2006**, *7*, 773–777.
- (31) Simth, M. E.; van Eck, E. R. H. Progress in Nuclear Magnetic Resonance Spectroscopy. *Prog. Nucl. Magn. Reson. Spectrosc.* **1999**, *34*, 159–201.
- (32) Rocha, J.; Morais, C. M.; Fernandez, C. Progress in Multiple-Quantum Magic-Angle Spinning NMR Spectroscopy. *Top. Curr. Chem.* **2005**, *246*, 141–196.
- (33) Medek, A.; Harwood, J. S.; Frydman, L. Multiple-Quantum Magic-Angle Spinning NMR: A New Method for the Study of Quadrupolar Nuclei in Solids. *J. Am. Chem. Soc.* **1995**, *117*, 12779–12787.
- (34) Fernandez, C.; Morais, C.; Rocha, J.; Pruski, M. High-Resolution Heteronuclear Correlation Spectra Between ³¹P and ²⁷Al in Microporous Aluminophosphates. *Solid State Nucl. Magn. Reson.* **2002**, *21*, 61–70.
- (35) Jung, H. J.; Shin, C.-H.; Hong, S. B. Si Distribution in Silicoaluminophosphate Molecular Sieves with the LEV Topology: A Solid-State NMR Study. *J. Phys. Chem. B* **2005**, *109*, 20847–20853.
- (36) Naonobu, K.; Nouno, K.; Lee, J. K.; Shin, J.; Hong, S. B.; Niwa, M. Acidic Properties of Cage-Based, Small-Pore Zeolites with Different Framework Topologies and Their Silicoaluminophosphate Analogues. *J. Phys. Chem. C* **2011**, *115*, 22505–22513.
- (37) Barthomeuf, D. Topology and Maximum Content of Isolated Species (Al, Ga, Fe, B, Si, ...) in a Zeolitic Framework. An Approach to Acid Catalysis. *J. Phys. Chem.* **1993**, *97*, 10092–10096.
- (38) Vomscheid, R.; Briend, M.; Peltre, M. J.; Man, P. P.; Barthomeuf, D. The Role of the Template in Directing the Si Distribution in SAPO Zeolites. *J. Phys. Chem.* **1994**, *98*, 9614–9618.
- (39) Shen, W.; Li, X.; Wei, Y.; Tian, P.; Feng, F.; Han, X.; Bao, X. A Study of the Acidity of SAPO-34 by Solid-State NMR Spectroscopy. *Microporous Mesoporous Mater.* **2012**, *158*, 19–25.
- (40) Chen, T. H.; Wouters, B. H.; Grobet, P. J. Enhanced Resolution of Al Sites in the Molecular Sieve SAPO-37 by ²⁷Al MQ MAS NMR. *Colloids Surf., A* **1999**, *158*, 145–49.
- (41) Jhung, S. H.; Hwang, Y. K.; Chang, J.; Park, S. Effect of Acidity and Anions on Synthesis of AFI Molecular Sieves in Wide pH Range of 3–10. *Microporous Mesoporous Mater.* **2004**, *67*, 151–157.
- (42) Liu, G.; Tian, P.; Liu, Z. Synthesis of SAPO-34 Molecular Sieves Templated with Diethylamine and Their Properties Compared with Other Templates. *Chim. J. Catal.* **2012**, *33*, 174–182.